

Transformer-Guided Deep Reinforcement Learning for Optimal Takeoff Trajectory Design of an eVTOL Drone

Nathan M. Roberts II^{*} and Xiaosong Du[†]

Missouri University of Science and Technology, Rolla, MO 65401

The rapid advancement of electric vertical take-off and landing (eVTOL) aircraft offers a promising opportunity to alleviate urban traffic congestion. Thus, developing optimal takeoff trajectories for minimum energy consumption becomes essential for broader eVTOL aircraft applications. Conventional optimal control methods (such as dynamic programming and linear quadratic regulator) provide highly efficient and well-established solutions but are limited by problem dimensionality and complexity. Deep reinforcement learning (DRL) emerges as a special type of artificial intelligence tackling complex, nonlinear systems; however, the training difficulty is a key bottleneck that limits DRL applications. To address these challenges, we propose the transformer-guided DRL to alleviate the training difficulty by exploring a realistic state space at each time step using a transformer. The proposed transformer-guided DRL was demonstrated on an optimal takeoff trajectory design of an eVTOL drone for minimal energy consumption while meeting takeoff conditions (*i.e.*, minimum vertical displacement and minimum horizontal velocity) by varying control variables (*i.e.*, power and wing angle to the vertical). Results presented that the transformer-guided DRL agent learned to take off with 4.57×10^6 time steps, representing 25% of the 19.79×10^6 time steps needed by a vanilla DRL agent. In addition, the transformer-guided DRL achieved 97.2% accuracy on the optimal energy consumption compared against the simulation-based optimal reference while the vanilla DRL achieved 96.3% accuracy. Therefore, the proposed transformer-guided DRL outperformed vanilla DRL in terms of both training efficiency as well as optimal design verification.

I. Introduction

ELECTRIC vertical take-off and landing (eVTOL) aircraft have emerged as an enabling technology for urban air mobility (UAM) [1–6]. UAM systems seek to alleviate urban congestion and improve transportation efficiency around and between metropolitan areas. The eVTOL aircraft are particularly well-suited for densely populated regions due to their precise control, low acoustic footprint, and environmental friendliness [7]. In response to fast-paced advancements in UAM and eVTOL technologies, the Federal Aviation Administration has been working to develop regulations and certifications for the use of drones and small aircraft—including eVTOL vehicles—in cities [8, 9], as recognition of and support for this new transportation concept.

Despite promising advancements, eVTOL technology also presents new challenges, among which the energy consumption (especially during the takeoff phase) becomes a key bottleneck. Optimal takeoff trajectory designs for eVTOL aircraft have been investigated to address the energy concerns [10–13]. Chauhan and Martins [14] performed multidisciplinary design optimization on the takeoff trajectory of an eVTOL aircraft to minimize energy use while maintaining passengers’ comfort with a maximum acceleration constraint. They also investigated the effects of constraints (*e.g.*, maximum angle of attack) on the optimal takeoff trajectories. NASA developed the Dymos [15] framework for the control of dynamic, multidisciplinary systems and included the reference [14] as a verification case.

Recently, there has been literature conducting artificial intelligence-enhanced optimal takeoff trajectory designs of eVTOL aircraft for higher efficiency. Sisk and Du [13] developed twin-generator generative adversarial networks to generate realistic eVTOL takeoff trajectories. The developed model facilitated surrogate modeling due to the generated realistic trajectories as well as the dimensionality reduction which further permitted efficient takeoff trajectory designs. Roberts and Du [16] developed a deep reinforcement learning (DRL) with an effective reward function formulation to learn the optimal takeoff policy. The trained policy achieved greater than 96% accuracy for optimal energy consumption and possessed flexibility for feedback control but suffered from high sample complexity.

^{*}Doctoral Student, Aerospace Engineering.

[†]Assistant Professor, Department of Mechanical and Aerospace Engineering, AIAA member.

Transformers are a family of neural network architectures developed for natural language processing tasks, where the attention-based mechanism performs well in translation and sequence understanding [17]. Unlike recurrent architectures (*e.g.*, recurrent neural networks and long short-term memory networks), transformers processes sequential data in parallel, efficiently learning long-range relationships using self-attention. The ability for a transformer to handle sequential data has led to applications beyond language processing, including time-series forecasting [18]. In this work, we train a transformer to represent the temporal changes in eVTOL control profiles. We use the trained transformer to guide a DRL agent operating in a complex, nonlinear environment. By integrating transformer-based sequential modeling with DRL, we aim to improve policy convergence and energy efficiency in eVTOL takeoff trajectories.

The remainder of this paper is organized as follows. In Sec. II, we detail the eVTOL simulation models. Also, we elaborate on the transformer architecture and DRL followed by the transformer-guided DRL. In III, we present the results achieved by the transformer-guided DRL, compared against simulation-based optimal reference and vanilla DRL-based results. We end this paper with conclusions and future work in Sec. IV

II. Methodology

A. eVTOL Models

The aircraft considered in this paper is a tandem, tilt-wing, eVTOL aircraft, which is modeled after the Airbus A³ Vahana [19]. Each wing has a rectangular planform with a span of 6 m, and a chord length of 1.5 m, using a NACA 0012 airfoil profile. Each wing has four three-bladed propellers with a radius of 0.75 m and a blade chord of 0.1 m. The front and rear wings are assumed to be geometrically identical and rotate in sync, balancing the pitch moments, removing the need to model trim and stability explicitly [14]. This symmetry reduces the degree of freedom to vertical and horizontal displacements only, which are measured with respect to a fixed inertial reference frame. The propeller thrust line is assumed to be in line with the wing chord. The body of the aircraft is assumed to have a drag area of 0.35 m², and the related drag coefficient does not vary with the angle of attack. The Dymos framework [15] developed by NASA is used to generate optimal design references.

1. Aerodynamics

Pre-stall aerodynamic coefficients are provided using finite-wing corrections with lifting-line theory. While transitioning from vertical to horizontal flight, a wing may experience stall conditions where linear aerodynamic assumptions are no longer valid. Lift and drag beyond the linear region must be available to accurately model this transition. Tangler and Ostowari [20] used experimental data to create an empirical model, estimating the post-stall lift coefficient (Eqn. (1)) and drag coefficient (Eqn. (5)) for a finite-length rectangular wing.

$$C_L = A_1 \sin(2\alpha) + A_2 \frac{\cos(\alpha)^2}{\sin(\alpha)}, \quad (1)$$

where

$$A_1 = \frac{C_1}{2}, \quad (2)$$

$$A_2 = (C_{L_s} - C_1 \sin(\alpha_s) \cos(\alpha_s)) \frac{\sin(\alpha_s)}{\cos(\alpha_s)^2}, \quad (3)$$

$$C_1 = 1.1 + 0.018AR, \quad (4)$$

α is the wing angle of attack, α_s is the angle of attack at the stall, C_{L_s} is the lift coefficient at stall, and AR is the wing aspect ratio. For post-stall angles of attack above 27.5 degrees, the drag coefficient is computed as follows.

$$C_D = B_1 \sin(\alpha) + B_2 \cos(\alpha), \quad (5)$$

where

$$B_1 = C_{D_{max}}, \quad (6)$$

$$B_2 = \frac{C_{D_s} - C_{D_{max}} \sin(\alpha_s)}{\cos(\alpha_s)}, \quad (7)$$

$$C_{D_{max}} = \frac{1.0 + 0.065AR}{0.9 + t/c}, \quad (8)$$

C_{D_s} represents the drag coefficient at stall, and t/c represents the thickness-to-chord ratio of the airfoil. For angles of attack below 27.5 degrees, the aerodynamic quantities experimentally gathered by Tangler and Ostowari [20] are used (Table 1). Tangler and Ostowari [20] showed that the airfoil geometry had a minimal effect on the post-stall characteristics, so the geometry is not included in Eqns. (1) and (5). Tangler and Ostowari [20] also showed that the Reynolds number has little effect on the post-stall characteristics within the range of 0.25×10^6 to 1×10^6 . This range is reasonable for the takeoff phase of the aircraft under consideration. Additionally, while the wings are assumed to be independent when calculating the lift and parasite drag, the induced drag is affected by aerodynamic interaction between the wings due to the tandem biplane configuration. Due to the wingtip motors, the span efficiency is assumed to be 0.95. The induced drag is determined as

$$D_{induced} = \frac{1}{\pi q} \left(2 \frac{L_{wing}^2}{b^2} + 2\sigma \frac{L_{wing}^2}{b^2} \right), \quad (9)$$

where q is the dynamic pressure and b is the span. For a gap-to-span ratio of 0.25, σ is approximately 0.4. This simplifies to the following, where it can be seen that the tandem wings reduce the span efficiency of both wings to 0.68, which is used to calculate the lift and drag for each wing independently.

$$D_{induced} = 2 \left(\frac{L_{wing}^2}{0.68 \cdot \pi \cdot q \cdot b^2} \right). \quad (10)$$

Since the lift and drag curves are not smooth where the models change, Kreisselmeier–Steinhauser (KS) functions are used to make them smooth to support gradient-based optimization.

Table 1 Drag coefficient data points between 16 and 27.5 degrees from Tangler and Ostowari [20].

α	16°	20°	25°	27.5°
C_D	0.100	0.175	0.275	0.363

2. Propulsion

The thrust, as a function of power provided, is calculated using momentum theory as follows.

$$P_{disk} = TV_{\infty\perp} + \kappa T \left(-\frac{V_{\infty\perp}}{2} + \sqrt{\frac{V_{\infty\perp}^2}{4} + \frac{T}{2\rho A_{disk}}} \right), \quad (11)$$

where P_{disk} represents the power supplied to the propeller disk, T represents the thrust, $V_{\infty\perp}$ represents the normal component of the freestream velocity, ρ represents the air density, A_{disk} represents the area of the propeller disk, and $\kappa = 1.2$ represents the correction factor accounting for nonuniform inflow, tip effects, and simplifications from momentum theory. The thrust must be solved numerically, since the power provided is a design variable. The Newton–Raphson method is applied with an initial guess of 1.2 times the weight of the aircraft.

The profile power can be estimated as

$$C_{P_p} = \frac{\sigma C_{d_{0p}}}{8} (1 + 4.6\mu^2), \quad (12)$$

where

$$\mu = \frac{V_{\infty\parallel}}{\Omega R}, \quad (13)$$

$$C_{P_p} = \frac{P_p}{\rho A_{disk} R^3 \Omega^3}, \quad (14)$$

where σ represents the solidity, C_{d0p} represents the constant profile drag coefficient, $V_{\infty\parallel}$ represents the parallel component of the freestream velocity, and C_{Pp} represents the coefficient of profile power. It is assumed that the propellers are variable-pitch and maintain a constant $\Omega = 181$ rad/s. The solidity is calculated to be 0.13, and C_{d0p} is assumed to be 0.012. The power supplied to the propeller disk can be calculated as follows $P_{disk} = \eta P_{electrical} - P_p$, with the supplied electric power as input. A loss factor η is used to account for mechanical and electrical losses.

The propellers will produce normal forces when the freestream flow is not aligned with the propeller axes. This force can be approximated using the empirical formula from Young [21] as follows:

$$N = \frac{4.25\sigma_e \sin(\beta + 8^\circ) f q_{\perp} A_{disk}}{1 + 2\sigma_e} \tan(\alpha_{in}), \quad (15)$$

where

$$\sigma_e = \frac{2Bc_b}{3\pi R}, \quad (16)$$

$$f = 1 + \frac{\sqrt{1 + T_c} - 1}{2} + \frac{T_c}{4(2 + T_c)}, \quad (17)$$

$$T_c = \frac{T}{q_{\perp} A_{disk}}, \quad (18)$$

β represents the blade pitch angle at three-quarters of the radius, q_{\perp} represents the dynamic pressure based on the normal component of the velocity, A_{disk} represents the propeller disk area, α_{in} represents the incidence angle, σ_e represents the effective solidity, B represents the number of blades per propeller, c_b represents the average blade chord, R represents the propeller radius, f represents the thrust factor, T_c represents the thrust coefficient, and T represents the thrust. β is assumed to change linearly from 0 to 35° as the flight speed increases from 0 to 67 m/s.

3. Propeller–Wing Interaction

Momentum theory is used to model the interaction between the induced flow from the propellers to the wings. Momentum theory finds a theoretical upper limit ($2v_i$) to the amount the flow speed can increase when it passes through a propeller disk. The induced velocity, v_i , can be computed as follows:

$$v_i = \left(-\frac{V_{\infty\perp}}{2} + 2\sqrt{\frac{V_{\infty\perp}^2}{4} + \frac{T}{2\rho A_{disk}}} \right). \quad (19)$$

Chauhan and Martins [14] calculated the propeller–wing interaction as $V_{\infty\perp} + k_w v_i$ and tested a range of k_w between 0 and 200%. They showed that the propeller–wing interactions had a negligible effect on the power required for takeoff. Therefore, we set $k_w = 1$ in this work.

4. Dynamics

The x and y components of the velocity at the next step are given by the following equations,

$$v_{x_{i+1}} = v_{x_i} + \frac{T_i \sin(\theta_i) - D_{fuse_i} \sin(\theta_i + \alpha_{\infty_i}) - D_{wings_i} \sin(\theta_i + \alpha_{EFS_i}) - L_{wings_i} \cos(\theta_i + \alpha_{EFS_i}) - N_i \cos(\theta_i)}{m} \delta t \quad (20)$$

and

$$v_{y_{i+1}} = v_{y_i} + \frac{T_i \cos(\theta_i) - D_{fuse_i} \cos(\theta_i + \alpha_{\infty_i}) - D_{wings_i} \cos(\theta_i + \alpha_{EFS_i}) - L_{wings_i} \sin(\theta_i + \alpha_{EFS_i}) + N_i \sin(\theta_i) - mg}{m} \delta t, \quad (21)$$

where i is the index of the time step, δt is the length of each time step, θ represents the wing angle relative to vertical, α_{∞} represents the freestream angle of attack, α_{EFS} represents the effective freestream angle of attack due to the propellers, m represents the mass of the aircraft, T represents the total thrust, D_{fuse} represents the drag of the fuselage, D_{wings} represents the total drag of both wings, L_{wings} represents the total lift of both wings, and N represents the total normal force from the propellers. The forward Euler method is used to propagate the aircraft states.

B. Transformer-Guided Deep Reinforcement Learning

1. Transformer

The transformer relies on a self-attention mechanism that enables each element in a sequence to attend to the other elements simultaneously, not relying on recurrence [17]. The parallel computation allows transformers to learn sequential or temporal relationships more efficiently than recurrent neural networks or long short-term memory (LSTM) networks which process sequences step by step. In this work, we extend the transformer to model the temporal evolution of control variables. The transformer is trained on optimal trajectories generated using Dymos, representing the underlying temporal patterns of the optimal control profiles.

The self-attention mechanism of transformers work by focusing on relevant portions of a sequence, while ignoring less relevant portions. Positional encoding integrates relative positions into a sequence. Relevance of one element in a sequence to other elements is determined using query, key, and value vectors. For a sequence of length n consisting of d -dimensional vectors $\mathbf{X} \in \mathbb{R}^{n \times d}$, the positional encoding is typically done using sine and cosine functions.

$$\mathbf{X}_{enc} = \mathbf{X} + \mathbf{PE}, \quad (22)$$

where

$$\begin{aligned} \mathbf{PE}_{pos,2i} &= \sin\left(\frac{pos}{10000^{\frac{2i}{d}}}\right), \\ \mathbf{PE}_{pos,2i+1} &= \cos\left(\frac{pos}{10000^{\frac{2i}{d}}}\right), \end{aligned}$$

pos is the position in the sequence, and i is the dimension. The query vector is how each element inquires the relevance of all elements—including itself—to itself. The query vector for an element is calculated by multiplying encoded sequence by a trainable weight matrix, $\mathbf{W}_q \in \mathbb{R}^{d \times d_k}$, where d_k is a hyperparameter.

$$\mathbf{q}_i = \mathbf{x}_{enc,i} \mathbf{W}_q \in \mathbb{R}^{1 \times d_k}. \quad (23)$$

Each element represents its relevance using a key vector, which is similarly calculated using a trainable weight matrix,

$$\mathbf{k}_i = \mathbf{x}_{enc,i} \mathbf{W}_k \in \mathbb{R}^{1 \times d_k}. \quad (24)$$

The value vector is created in the same manner, and represents the information a particular element can offer.

$$\mathbf{v}_i = \mathbf{x}_{enc,i} \mathbf{W}_v \in \mathbb{R}^{1 \times d_k}. \quad (25)$$

An attention vector is calculated for an element by taking the dot product of the query vector with every key vector, measuring the compatibility of the query and key vectors.

$$\mathbf{a}_i = \text{softmax}\left(\frac{[\mathbf{q}_i^\top \mathbf{k}_1, \mathbf{q}_i^\top \mathbf{k}_2, \dots, \mathbf{q}_i^\top \mathbf{k}_n]}{\sqrt{d_k}}\right)^\top \in \mathbb{R}^{1 \times n}. \quad (26)$$

Elements of an attention vector will be close to zero if the corresponding key vectors are dissimilar to the query vector—meaning the corresponding vector of sequence \mathbf{X}_{enc} is irrelevant to $\mathbf{x}_{enc,i}$ —and close to one if they are similar. The output of the attention mechanism is a weighted sum of the value vectors, using an element’s attention vector as the weights,

$$\mathbf{z}_i = \sum_{j=1}^n \mathbf{a}_{ij} \mathbf{v}_j \in \mathbb{R}^{1 \times d_k}. \quad (27)$$

In practice, the attention mechanism is simultaneously run for many queries which are stacked into \mathbf{Q} , with the keys and values becoming \mathbf{K} and \mathbf{V} respectively. The matrix of outputs is then computed as

$$\text{Attention}(\mathbf{Q}, \mathbf{K}, \mathbf{V}) = \text{softmax}\left(\frac{\mathbf{Q}\mathbf{K}^\top}{\sqrt{d_k}}\right) \mathbf{V} \in \mathbb{R}^{n \times d_k}. \quad (28)$$

In applications where the transformer will be generating one element at a time, as is the case in this work, it is important to prevent later elements in a trajectory from being attended to. This is done while calculating the attention matrix by masking out the inputs to the softmax containing unwanted connections as shown in Eqn. 29.

$$A = \text{softmax} \left(\frac{QK^\top}{\sqrt{d_k}} + M \right), \quad (29)$$

where the mask is a strictly upper triangular matrix of size n ,

$$M = \begin{bmatrix} 0 & -\infty & -\infty & \cdots & -\infty \\ 0 & 0 & -\infty & \cdots & -\infty \\ 0 & 0 & 0 & \cdots & -\infty \\ \vdots & \vdots & \vdots & \ddots & \vdots \\ 0 & 0 & 0 & \cdots & 0 \end{bmatrix} \in \mathbb{R}^{n \times n}.$$

To capture multiple representations or underlying relationships, it is common to perform multiple separate attention operations on the same set of queries, keys, and values. Multi-head attention projects the queries, keys, and values with additional learnable matrices, then attends to each of the projections, and linearly combines the outputs.

$$\text{MultiHead}(Q, K, V) = \text{Concat}(\text{head}_1, \text{head}_2, \dots, \text{head}_h) W_O \in \mathbb{R}^{n \times d_v}, \quad (30)$$

where

$$\text{head}_i = \text{Attention}(QW_{Q,i}, KW_{K,i}, VW_{V,i}).$$

$W_{Q,i}, W_{K,i} \in \mathbb{R}^{d \times d_k}$, $W_{V,i} \in \mathbb{R}^{d \times d_v}$, and $W_O \in \mathbb{R}^{d_v \times h \times d}$ are learnable parameters, while the value dimension d_v and number of heads h are hyperparameters.

In this study, an encoder-only transformer is trained on optimal control trajectories to learn the temporal relations within the optimal control profiles. Each training step is conducted as follows:

- 1) A batch of trajectories are pulled from the training set.
- 2) Because the trajectories have low-dimensional elements (*i.e.*, two control actions at each time step in this work), they are projected into a higher-dimensional space using a single-layer feed-forward neural network (FNN) such that $d = d_k = d_v = 64$.
- 3) The projected trajectories are positionally embedded following the procedure described in Eqn. 22.
- 4) The embedded trajectories are passed through two masked multi-head self-attention layers.
- 5) The attention outputs are passed through another single-layer FNN to create distribution parameters: mean μ and variance σ^2 .
- 6) The negative log-likelihood (Eqn. 31) of producing the next element under the distribution described by the parameters serves as a loss function,

$$\mathcal{L}_{\text{NLL}} = \frac{1}{2N} \sum_{i=1}^N \sum_{j=1}^D \left[\ln(2\pi\sigma_{i,j}^2) + \frac{(y_{i,j} - \mu_{i,j})^2}{\sigma_{i,j}^2} \right], \quad (31)$$

where N is the total number of samples in the batch, and D is the dimensionality of the sequence elements.

- 7) The Adam optimizer takes one step.

2. Deep Reinforcement Learning

Reinforcement learning (RL) is an artificial intelligence method through which an agent interacts with an environment, learning to execute optimal actions on any given states, with the goal of maximizing cumulative rewards over an episode [22]. RL is modeled as a Markov decision process, which consists of a set of possible states S , called the state space, a set of possible actions A , called the action space, the probability $P_a(s, s')$ of transitioning from state s to state s' given action a , and the reward $R_a(s, s')$ for taking action a to transition from state s to s' .

An RL agent acting at time t takes the current state S_t as input, and samples action A_t from the learned distribution $\pi(S_t)$. The state then transitions to S_{t+1} with probability $P(S_{t+1}|A_t, S_t)$, and a reward R_{t+1} is received. The policy π is a mapping of the state space to the action space as follows,

$$\pi(s) = P(A_t | S_t = s). \quad (32)$$

The agent aims to learn the optimal policy $\pi^*(s)$ that maximizes the cumulative reward, $\sum_{t=1}^N R_t$, over N time steps. RL that uses deep neural networks to learn this mapping is known as DRL.

In this work, we use the soft actor-critic (SAC) method [23], in which a policy network (termed actor) selects actions while critic networks (termed critic) evaluate how good those actions are by estimating the value which is the sum of the immediate reward and cumulative future rewards. The value networks in the critic predict the expected return of being in state s (*i.e.*, state value), while Q-networks predicts the expected return of taking action a in state s (*i.e.*, action value). The critic delivers a temporal difference error to the actor after each action, representing the difference between the expected and observed reward for the next state. A unique feature of SAC, compared with universal actor-critic methods, is the inclusion of an entropy regularization term into the loss function for training the policy [24]

$$L = -Q(\tilde{a}_\theta(s), s) + \alpha \log \pi_\theta(\tilde{a}_\theta(s) | s), \quad (33)$$

where $Q(\tilde{a}_\theta(s), s)$ is the action value predicted by the Q-network, α is an entropy-regularization parameter, and $a_\theta(s)$ is an action sampled from $\pi_\theta(s)$. Entropy, which quantifies the randomness of a probability distribution, is used to encourage exploration by promoting stochasticity in the policy. Importantly, SAC operates off-policy, meaning that the data used to train the networks does not need to be generated by the current policy. Instead, experiences collected from previous iterations of the policy can still contribute to improving the performance of the actor and critic networks.

The SAC agent in this work is trained for 5×10^6 time steps, implemented via the `Stable Baselines3` library [25]. The agent is evaluated every 1×10^4 steps to save the model with the highest cumulative reward. Both the actor and critic networks are composed of three fully connected layers, each containing 512 neurons and employing the ReLU activation function. Training is conducted using a linearly-annealed learning rate starting at 4×10^{-4} , a batch size of 256, a soft target update coefficient of 5×10^{-3} , a discount factor of 0.98, and an entropy coefficient of 0.01. To mitigate issues such as catastrophic forgetting and policy collapse, the agent utilized a replay buffer capable of storing up to 5×10^6 elements.

3. Transformer-guided Deep Reinforcement Learning

DRL has a key drawback, requiring large amounts of data or many simulations to be trained. Environments with strict constraints or early termination criteria are particularly prone to this issue. eVTOL takeoff trajectory design, due to the dangers inherent in air travel, necessitates such an environment. To address the training difficulty, we propose the transformer-guided DRL for optimal takeoff trajectory design in this work.

The transformer-guided DRL (Fig. 1) selects an action from a distribution that the trained transformer generates while vanilla DRL learns to take actions within a pre-defined space which typically incurs the training difficulty. Specifically, the transformer produces an action proposal distribution characterized by a mean and variance for each action component, conditioned on the previous action history. The action proposal distribution sets up the DRL state space at each time step, and the agent generates a value within $[-1, 1]$, corresponding to the z-score of the action from the distribution that is to be executed. This range, $[-1, 1]$, is chosen because it captures the majority of the distribution while keeping the executed action near the mean. This method substantially reduces the effective exploration space.

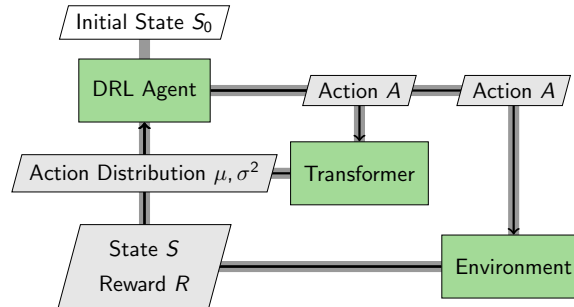


Fig. 1 The training loop of a transformer-guided DRL agent.

After each time step, the executed action is appended to the action history, which is then used by the transformer to generate the next action proposal distribution. Because the action proposal distribution is distinct from the executed

action, a traditional encoder-decoder transformer architecture is not feasible. Appending the action distribution parameters to the state space allows the policy to account for previous actions, interpreted through the lens of the transformer. To allow the DRL agent to select the first action, the initial state from the environment is appended with a start token outside the transformer’s output range. This allows the agent to determine the starting point from which the transformer guides.

III. Results and Discussion

A. Problem Formulation

The optimal takeoff trajectory design problem is formulated for minimum energy consumption with constraints on takeoff conditions (Table 2). Specifically, we define takeoff as reaching an altitude of at least 305 m with a horizontal velocity of at least 67 m/s. The aircraft cannot go through solid ground, so the altitude has a lower bound of 0 meters. The design variables include 40 B-spline points (*i.e.*, 20 for power control profile and 20 for wing angle control profile) and the total takeoff time. The reference results are generated using Dymos [15].

Table 2 Takeoff trajectory optimization problem formulation.

	Function or Variable	Description	Quantity
minimize	E	Electrical energy consumed	
w.r.t.	\mathbf{P}	Electrical power	20
	θ	Wing angle to vertical	20
	T_{takeoff}	Total takeoff time	1
		Total design variables	41
subject to	$y_{\text{final}} \geq 305 \text{ m}$	Final vertical displacement constraint	1
	$v_{x,\text{final}} \geq 67 \text{ m/s}$	Final horizontal speed constraint	1
	$y \geq 0 \text{ m}$	Vertical displacement constraint	1
		Total constraints	3

B. Transformer-Guided Deep Reinforcement Learning

The transformer is trained on 1,000 reference optimal trajectories [26] gathered via Latin hypercube sampling for five flight condition parameters (Table 3). Specifically, 750 samples are used to train the transformer, 150 are used as validation data, and 100 are used as testing data. Each of the trajectories is interpolated into 0.1 second intervals using cubic splines, following the process Dymos uses for time-series outputs. The transformer is trained based on the true next element under the generated distribution (Sec. II.B). In the verification case, we use $k_w = 1$, $\eta = 0.9$, and $S_{\text{ref}} = 1$, with only takeoff conditions as shown in Table 2.

Table 3 Flight-condition space used for generating training optimal trajectories for a transformer. The parameters with subscripts "max" denote corresponding upper bounds.

Quantity	α_{max}	a_{max}	k_w	η	S_{ref}
Description	acceleration	angle of attack	induced velocity factor	efficiency factor	wing planform area scale
Range	$[10, 15]^\circ$	$[0.2, 0.4] \text{ g}$	$[0.3, 1]$	$[0.7, 0.9]$	$[0.9, 1]$

The encoder-only transformer used in this work has an input dimension D of 2, a hidden dimension $d_k = d_v$ of 64, 4 attention heads, and 2 attention layers, and utilizes a dropout of 0.1 during training. The model is trained using the Adam optimizer with a learning rate of 10^{-4} and batch size of 64 for 100 epochs. The best model is saved according to the validation data. We use the best model auto-regressively generate trajectories starting from the first action of each of the testing trajectories to evaluate the transformer’s ability to generate a realistic or suboptimal trajectory. The

trained transformer achieved 95.4% accuracy (formulated as follows) on energy consumption compared with the testing trajectories.

$$RA = 1 - \frac{|E_{\text{generated}} - E_{\text{reference}}|}{E_{\text{reference}}} \quad (34)$$

In this work, we develop a DRL-compatible environment, containing the simulation models, optimization objective, and takeoff conditions, using the `Gymnasium` interface in `python` [27]. At the core of DRL lies the reward function, which leads the behavior of the agent. At each time step within the developed environment, the agent gets feedback composed of several reward components (Table 4). The relative weight afforded to each portion of the reward is governed by the hyperparameter $\rho = 2$. To lead the agent toward takeoff, the reward includes a penalty based on the difference between the current state and the target takeoff state. For effective guidance, these reward components are formulated as convex shapes with singularities [28], with concavity governed by a concavity coefficient hyperparameter $cc = 0.5$. Energy efficiency is promoted by penalizing energy consumption at each time step, encouraging a minimum-energy trajectory. All rewards are scaled using scale hyperparameter $k = 0.05$. The negative reward structures incentivize the agent to terminate the episode as soon as possible, which occurs if the agent violates any physical constraints, exceeds the time limit, or successfully takes off. To prevent the agent from exploiting early termination through constraint violation, the unweighted maximum future energy penalty, $R_{P,\text{max}}(t) = -10k(t_{\text{max}} - t)$, is applied if a flight constraint is violated. The early termination conditions include hitting the ground or generating a negative freestream velocity.

Table 4 Reward components.

Quantity	R_y	R_{V_x}	R_P
Value	$\frac{ke^{cc} \left(e^{-cc} \left 1 - \frac{y}{305} \right - 1 \right)}{3(e^{cc} - 1)(\rho + 1)}$	$\frac{ke^{cc} \left(e^{-cc} \left 1 - \frac{V_x}{67} \right - 1 \right)}{3(e^{cc} - 1)(\rho + 1)}$	$\frac{-\rho k P}{310000(\rho + 1)}$

The state space is comprised of altitude, horizontal velocity, vertical velocity, mean power, mean wing angle, power variance, and wing angle variance (Table 5). These quantities are selected because they directly affect the reward function and relate to the early termination conditions. By only including quantities that are critical to the reward function and termination, the agent is able to focus on the most relevant aspects of the task. To ensure the agent begins each episode from a feasible state, the initial conditions include a small vertical velocity and displacement. The agent alone predicts the first action that is executed and used to initialize the transformer-generated sequence. Because the transformer is not initialized by the first step, the distribution parameters are not present, and their position in the state is padded with sevens.

Table 5 DRL agent state space.

Quantity	Description	Initial Value
y	Altitude	0.1 m
V_x	Horizontal Velocity	0.1 m/s
V_y	Vertical Velocity	0.1 m/s
μ_P	Mean Power	7
μ_θ	Mean Wing Angle	7
σ_P^2	Variance of Power	7
σ_θ^2	Variance of Wing Angle	7

The action space (Table 6) contains the power provided to the motors and the wing angle to the vertical. The action space of the DRL agent differs from the action space of the DRL environment. In vanilla DRL, the two action spaces are identical, but as mentioned in Sec. II.B, the transformer-guided DRL agent’s action space corresponds to the z-scores of the actions to be executed from the transformer’s action distribution. The executed actions are analogous to the design variables described in Table 2. Time is not directly predicted in DRL, but the environment operates on a time step of 0.1 seconds with a maximum episode length of 40 seconds.

Table 6 DRL environment action space, consisting of power (P) and wing angle to the vertical (θ).

Quantity	P	θ
Range	$[1.8, 3.11] \times 10^5 \text{W}$	$[0, \frac{\pi}{2}] \text{ rad}$

C. Verification

The reference trajectory generated using Dymos consumes 1,693W h over a duration of 19.6 s. All optimal trajectories (*i.e.*, reference, vanilla DRL, and transformer-guided DRL) satisfy all takeoff conditions, achieving an altitude of 305 m (Fig. 2a) and a horizontal velocity of 67 m/s (Fig. 2b). The trajectory produced by a previous DRL agent trained by Roberts and Du [16] consumes 1,759W h over a duration of 21.4 s. In comparison, the trained transformer-guided DRL agent identifies a trajectory consuming 1,740W h over a duration of 21.5 s. Moreover, the transformer-guided DRL agent learns to take off with 4.57×10^6 time steps while the vanilla DRL takes 19.79×10^6 time steps. Despite using only one fourth as many time steps of vanilla DRL, the transformer-guided DRL trajectory exhibits 97.2% accuracy in the minimum energy consumption compared against the Dymos solution (Table 7).

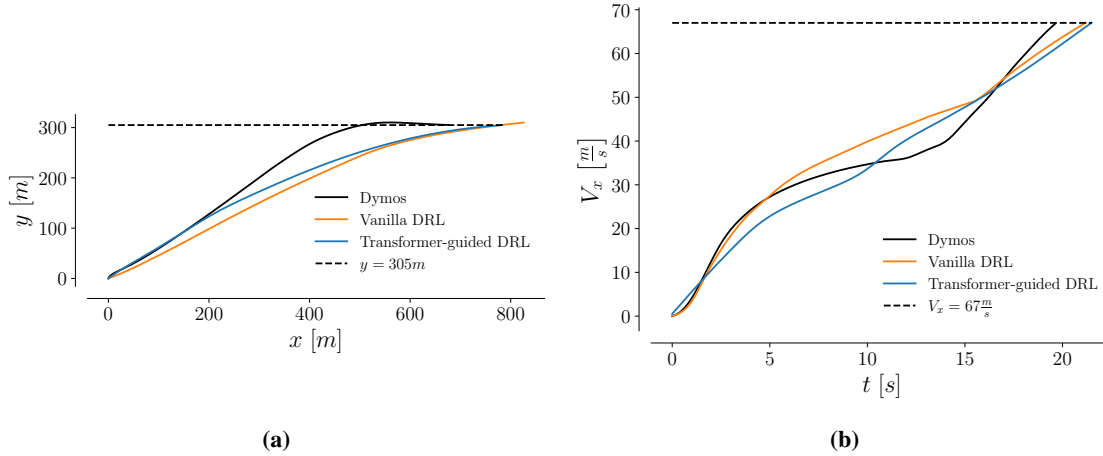


Fig. 2 Comparison of takeoff trajectories: (a) optimal trajectories; (b) horizontal velocity during takeoff.

Table 7 Accuracy on energy consumption for optimized trajectories.

	Vanilla DRL	Transformer-guided DRL
Accuracy	96.1%	97.2%

IV. Conclusion and Future Work

Urban air mobility has emerged as a promising solution to alleviate urban congestion, with electric vertical takeoff and landing (eVTOL) aircraft offering quiet and efficient operation in densely populated environments. A central challenge limiting the widespread deployment of eVTOL aircraft is their high energy demand, particularly during takeoff, which consumes a disproportionate fraction of total energy. As a result, the design of minimal-energy takeoff trajectories is of substantial interest. Conventional optimal control methods often struggle with high-dimensional, nonlinear dynamics, while deep reinforcement learning (DRL) can handle such difficulties but typically suffers from training difficulty.

In this work, we developed a transformer-guided DRL framework for optimal takeoff trajectory design of an eVTOL aircraft. The proposed approach used the sequential-modeling capacity of a transformer—originally developed for machine translation tasks—to guide a DRL agent toward efficient takeoff while alleviating the training complexity

which is often encountered in constrained DRL environments. The transformer, trained on optimal takeoff trajectories for a range of flight conditions, reduced the action space to a more realistic and energy-efficient manifold.

The proposed transformer-guided DRL approach attained an optimal takeoff trajectory with at least 97% accuracy on energy consumption relative to a Dymos reference solution. Compared to vanilla DRL, the method required only one quarter of the training samples to converge, and achieved superior accuracy in minimal energy consumption. These results demonstrated that incorporating a learned temporal structure into the DRL process improved the training efficiency and the learned policy quality.

Future work will evaluate the framework under a range of flight conditions, and incorporate additional path and safety constraints. Further research will also consider alternative DRL or transformer designs. The integration of transformer-based sequential modeling with DRL presents a promising pathway toward data-efficient dynamic control strategies for eVTOL trajectories.

References

- [1] Tripaldi, F., Vianello, S., and Bianchi, N., “Emerging Trends in Urban Air Mobility: An Extensive Review,” *Energies*, Vol. 18, No. 6, 2025, p. 1426.
- [2] *Fast-Forwarding to a Future of On-Demand Urban Air Transportation*, Uber Elevate, October 2016. URL https://d1nyezh1ys8wfo.cloudfront.net/static/PDFs/Elevate%2BWhitepaper.pdf?uclid_id=a12a5e10-ccfe-4b20-b2b7-b13a6485bd26.
- [3] *Concept of Operations for Uncrewed Urban Air Mobility*, Boeing, 2023. URL <https://wisk.aero/conops/>.
- [4] *UTM Concept of Operations Version 2.0 (UTM ConOps v2.0)*, FAA, 2020. URL <https://www.faa.gov/researchdevelopment/trafficmanagement/utm-concept-operations-version-20-utm-conops-v20>.
- [5] Wild, G., “Urban Aviation: The Future Aerospace Transportation System for Intercity and Intracity Mobility,” *Urban Science*, Vol. 8, No. 4, 2024. <https://doi.org/10.3390/urbansci8040218>, URL <https://www.mdpi.com/2413-8851/8/4/218>.
- [6] Zhou, Q., and Tan, F., “Avionics of Electric Vertical Take-off and Landing in the Urban Air Mobility: A Review,” *IEEE Aerospace and Electronic Systems Magazine*, 2024, pp. 1–26. <https://doi.org/10.1109/MAES.2024.3488655>.
- [7] André, N., and Hajek, M., “Robust environmental life cycle assessment of electric VTOL concepts for urban air mobility,” *AIAA aviation 2019 forum*, 2019, p. 3473.
- [8] *Advisory Circular, Subject: Type Certification—Powered-lift, AC No: 21.17-4*, United States Department of Transportation, Federal Aviation Administration, July 2025.
- [9] Thomson, K., “FAA Drone and AAM Symposium Remarks,” FAA Drone and AAM Symposium, Baltimore, Maryland, July 30 2024.
- [10] Wang, M., Chu, N., Bhardwaj, P., Zhang, S., and Holzapfel, F., “Minimum-Time Trajectory Generation of eVTOL in Low-Speed Phase: Application in Control Law Design,” *IEEE Transactions on Aerospace and Electronic Systems*, Vol. 59, No. 2, 2023, pp. 1260–1275. <https://doi.org/10.1109/TAES.2022.3198033>.
- [11] Wei, H., Lou, B., Zhang, Z., Liang, B., Wang, F.-Y., and Lv, C., “Autonomous Navigation for eVTOL: Review and Future Perspectives,” *IEEE Transactions on Intelligent Vehicles*, Vol. 9, No. 2, 2024, pp. 4145–4171. <https://doi.org/10.1109/TIV.2024.3352613>.
- [12] Yeh, S.-T., and Du, X., “Transfer-Learning-Enhanced Regression Generative Adversarial Networks for Optimal eVTOL Takeoff Trajectory Prediction,” *Electronics*, Vol. 13, No. 10, 2024, p. 1911.
- [13] Sisk, S., and Du, X., “Surrogate-Based Multidisciplinary Optimization for the Takeoff Trajectory Design of Electric Drones,” *Processes*, Vol. 12, No. 9, 2024. <https://doi.org/10.3390/pr12091864>, URL <https://www.mdpi.com/2227-9717/12/9/1864>.
- [14] Chauhan, S. S., and Martins, J. R., “Tilt-wing eVTOL takeoff trajectory optimization,” *Journal of Aircraft*, Vol. 57, No. 1, 2020, pp. 93–112.
- [15] Falck, R., Gray, J. S., Ponnappalli, K., and Wright, T., “dymos: A Python package for optimal control of multidisciplinary systems,” *Journal of Open Source Software*, Vol. 6, No. 59, 2021, p. 2809. <https://doi.org/10.21105/joss.02809>, URL <https://doi.org/10.21105/joss.02809>.

- [16] Roberts, N. M., and Du, X., *Deep Reinforcement Learning for Optimal Takeoff Trajectory Design of an eVTOL Drone*, American Institute of Aeronautics and Astronautics, inc., 2025. <https://doi.org/10.2514/6.2025-3800>, URL <https://arc.aiaa.org/doi/abs/10.2514/6.2025-3800>.
- [17] Vaswani, A., Shazeer, N., Parmar, N., Uszkoreit, J., Jones, L., Gomez, A. N., Kaiser, L., and Polosukhin, I., “Attention is all you need,” *Proceedings of the 31st International Conference on Neural Information Processing Systems*, Curran Associates Inc., Red Hook, NY, USA, 2017, p. 6000–6010.
- [18] Wen, Q., Zhou, T., Zhang, C., Chen, W., Ma, Z., Yan, J., and Sun, L., “Transformers in time series: A survey,” *arXiv preprint arXiv:2202.07125*, 2022.
- [19] Airbus, “Vahana,” , 2016. URL <https://acubed.airbus.com/blog/vahana/>, [Online; accessed in 2025].
- [20] Tangler, J. L., and Ostowari, C., “Horizontal axis wind turbine post stall airfoil characteristics synthesization,” Tech. rep., Solar Energy Research Inst., Golden, CO (United States), 1991.
- [21] Young, J. D., “Propeller at high incidence,” *Journal of Aircraft*, Vol. 2, No. 3, 1965, pp. 241–250.
- [22] Kaelbling, L. P., Littman, M. L., and Moore, A. W., “Reinforcement learning: a survey,” *J. Artif. Int. Res.*, Vol. 4, No. 1, 1996, p. 237–285.
- [23] Haarnoja, T., Zhou, A., Abbeel, P., and Levine, S., “Soft Actor-Critic: Off-Policy Maximum Entropy Deep Reinforcement Learning with a Stochastic Actor,” , 2018. URL <https://arxiv.org/abs/1801.01290>.
- [24] OpenAI, “Soft Actor-Critic,” , 2018. URL <https://spinningup.openai.com/en/latest/algorithms/sac.html>, accessed online, 2025.
- [25] Raffin, A., Hill, A., Gleave, A., Kanervisto, A., Ernestus, M., and Dormann, N., “Stable-Baselines3: Reliable Reinforcement Learning Implementations,” *Journal of Machine Learning Research*, Vol. 22, No. 268, 2021, pp. 1–8. URL <http://jmlr.org/papers/v22/20-1364.html>.
- [26] Yeh, S.-T., and Du, X., “Optimal Tilt-Wing eVTOL Takeoff Trajectory Prediction Using Regression Generative Adversarial Networks,” *Mathematics*, Vol. 12, No. 1, 2023. <https://doi.org/10.3390/math12010026>, URL <https://www.mdpi.com/2227-7390/12/1/26>.
- [27] Towers, M., Kwiatkowski, A., Terry, J., Balis, J. U., Cola, G. D., Deleu, T., Goulão, M., Kallinteris, A., Krimmel, M., KG, A., Perez-Vicente, R., Pierré, A., Schulhoff, S., Tai, J. J., Tan, H., and Younis, O. G., “Gymnasium: A Standard Interface for Reinforcement Learning Environments,” , 2025. URL <https://arxiv.org/abs/2407.17032>.
- [28] Huang, B., and Jin, Y., “Reward shaping in multiagent reinforcement learning for self-organizing systems in assembly tasks,” *Advanced Engineering Informatics*, Vol. 54, 2022, p. 101800. <https://doi.org/https://doi.org/10.1016/j.aei.2022.101800>, URL <https://www.sciencedirect.com/science/article/pii/S1474034622002580>.